Testing the diffusing boundary model for the helix–coil transition in peptides

Sabine Neumaier, Andreas Reiner[1], Maren Büttner, Beat Fierz[2], and Thomas Kiefhaber[3]

Munich Center for Integrated Protein Science and Department of Chemistry, Technische Universität München, D-85747 Garching, Germany

Edited* by Robert L. Baldwin, Stanford University, Stanford, CA, and approved June 26, 2013 (received for review February 25, 2013)

The dynamics of peptide α-helices have been studied extensively for many years, and the kinetic mechanism of the helix–coil dynamics has been discussed controversially. Recent experimental results have suggested that equilibrium helix–coil dynamics are governed by movement of the helix/coil boundary along the peptide chain, which leads to slower unfolding kinetics in the helix center compared with the helix ends and position-independent helix formation kinetics. We tested this diffusion of boundary model in helical peptides of different lengths by triplet-triplet energy transfer measurements and compared the data with simulations based on a kinetic linear Ising model. The results show that boundary diffusion in helical peptides can be described by a classical, Einstein-type, 1D diffusion process with a diffusion coefficient of $2.7{\cdot}10^7$ (amino acids)^2/s or $6.1{\cdot}10^{-9}$ cm^2/s. In helices with a length longer than about 40 aa, helix unfolding by coil nucleation in a helical region occurs frequently in addition to boundary diffusion. Boundary diffusion is slowed down by helix-stabilizing capping motifs at the helix ends in agreement with predictions from the kinetic linear Ising model. We further tested local and nonlocal effects of amino acid replacements on helix–coil dynamics. Single amino acid replacements locally affect folding and unfolding dynamics with a ϕ_f-value of 0.35, which shows that interactions leading to different helix propensities for different amino acids are already partially present in the transition state for helix formation. Nonlocal effects of amino acid replacements only influence helix unfolding ($\phi_f = 0$) in agreement with a diffusing boundary mechanism.

α-helix capping | ϕ-value | protein folding

Folding and unfolding dynamics of α-helices play a prominent role in folding and other physiologically important conformational transitions in proteins. In polyalanine-based model peptides, the structure and dynamics of α-helices can be investigated in the absence of tertiary interactions, which yields information on intrinsic helix properties (1). Experimental and theoretical work has showed that a linear Ising model is able to describe the equilibrium properties of the helix–coil transition both in long homopolymers and in short model peptides (2–7). The kinetic mechanism of helix–coil dynamics has long been under debate. Temperature jump-induced unfolding experiments on short Ala-based helices showed that global unfolding occurs on the hundreds of nanoseconds time scale (8, 9). In a previous study, we applied triplet-triplet energy transfer (TTET) to investigate local folding and unfolding dynamics at different positions in a 21-aa Ala-based α-helix at equilibrium (10). The results revealed a position-independent helix elongation time constant ($1/k_f$) of about 400 ns at 5 °C and a position-dependent helix unfolding rate constant ($1/k_u$) with faster unfolding at the termini ($1/k_u = 250$ ns) compared with the center ($1/k_u = 1.4$ μs). This behavior could be reproduced in simulations using a kinetic version of the linear Ising model (10, 11), which suggested that helix elongation and unfolding mainly occur via a diffusing boundary mechanism (i.e., by the movement of the helix/coil boundary along the polypeptide chain). Helix nucleation in a completely unfolded chain and coil nucleation within a helical region are rare events in short model helices (10). The helix/coil boundary is statistically more likely located near the peptide ends than near the center (6, 10). Thus, it takes, on average, longer for the moving helix/coil boundary to reach the helix center than the helix ends, which leads to the observed position dependence of helix unfolding.

Here, we use TTET to test the diffusing boundary mechanism and to investigate whether diffusion of the helix/coil boundary along the polypeptide chain can be described by a classical, Einstein-type, 1D diffusion process. We further tested for local and nonlocal effects of changes in helix stability on folding and unfolding dynamics in different regions of α-helical peptides. The triplet donor xanthonic acid (Xan) and the acceptor 1-naphthylalanine (Nal) were attached to helical peptides in i, i + 6 spacing, which places them on opposing sides of the helix and prevents TTET in the helical state (10) (H; Fig. 1). When the helical structure between the labels is unfolded or partially unfolded (C conformations; Fig. 1), TTET can occur by van der Waals contact to the state C*. Because TTET between these groups is an irreversible process (12–14), the overall reaction can be described by the three-state model shown in Fig. 1. If helix–coil dynamics (k_f and k_u) and loop formation in the unfolded state occur on a similar time scale, the observable rate constants for TTET and their corresponding amplitudes yield the rate constants for local helix formation and unfolding between the labels, k_f and k_u, as well as the rate constant for loop formation (k_c) (10) (*SI Text*). In addition, the local equilibrium constant (K_{eq}) for helix formation in the region of the labels can be calculated from $K_{eq} = k_f / k_u$. It should be noted that TTET experiments do not require perturbation of the helix–coil equilibrium, and thus yield information on equilibrium fluctuations of the system.

Our results show that boundary diffusion in helical peptides can be described by a classical, 1D diffusion process. Nonlocal effects of changes in helix stability exclusively affect the dynamics of helix unfolding, whereas helix formation is unchanged. Locally, in contrast, changes in helix stability alter both folding and unfolding dynamics, with a ϕ_f-value (see Eq. **3**) of about 0.35.

Results and Discussion

Effect of Peptide Length on Helix Folding and Unfolding Dynamics. As in our previous work (10), we studied Ala-based helical peptides with Arg residues introduced with i, i + 5 spacing to increase solubility (1), which yields the canonical sequence Ac-AAAAA$(AAARA)_n$A-NH_2. Labels were inserted with i, i + 6 spacing, which prevents TTET in the helical state (Fig. 1). The triplet donor 9-oxoxanthene-2 carboxylic acid (Xan) was attached to the side chain of the nonnatural amino acid α,β-diaminopropionic

Author contributions: S.N., A.R., B.F., and T.K. designed research; S.N., A.R., M.B., and B.F. performed research; S.N., A.R., M.B., B.F., and T.K. analyzed data; and S.N. and T.K. wrote the paper.

The authors declare no conflict of interest.

*This Direct Submission article had a prearranged editor.

Freely available online through the PNAS open access option.

[1]Present address: Department of Molecular and Cell Biology, University of California, Berkeley, CA 94720.

[2]Present address: Laboratory of Biophysical Chemistry of Macromolecules, École Polytechnique Fédérale de Lausanne, CH-1015 Lausanne, Switzerland.

[3]To whom correspondence should be addressed. E-mail: t.kiefhaber@tum.de.

This article contains supporting information online at www.pnas.org/lookup/suppl/doi:10.1073/pnas.1303515110/-/DCSupplemental.

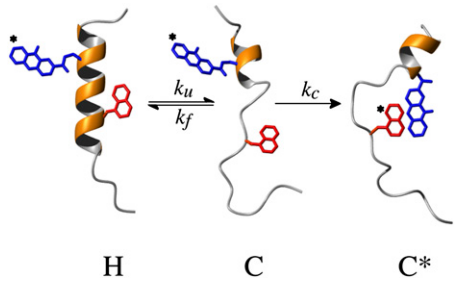

Fig. 1. Schematic representation of TTET coupled to a helix–coil equilibrium. The triplet labels Xan (blue) and Nal (red) are placed in the helix with i, i + 6 spacing.

acid (Dpr) via an amide bond, and the nonnatural amino acid Nal was introduced as triplet acceptor (Figs. 1 and 2).

Our previous results suggested that the experimentally observed position dependence of helix formation and unfolding dynamics originates in a boundary diffusion mechanism that can be described by a kinetic linear Ising model (10, 11) (a detailed description of the model is provided in *SI Text*). The boundary diffusion model predicts that the unfolding rate constant in the center of a helix is sensitive to helix length due to varying boundary diffusion distances. Unfolding at the termini and helix formation, in contrast, should be independent of helix length. To test this prediction, we synthesized helical peptides of different lengths between 16 and 41 aa and placed the TTET labels either in the center of the peptide or at the N terminus (Fig. 2 *A* and *E*). Shorter peptides did not form helices that are stable enough to yield reliable results on k_u and k_f. The far-UV CD spectra of all peptides display typical helical bands, with a maximum of the ellipticity at 190 nm and minima at 208 nm and 222 nm (Fig. 2 *B* and *F*). A quantitative analysis of the helix content using the signal at 222 nm would be inaccurate because the TTET labels have CD bands in the far-UV region. The increase in the strength of the CD band at 222 nm with increasing peptide length (Fig. 2 *B* and *F* and Table S1) indicates a higher average helical content, and thus, on average, longer helices in longer peptides in agreement with previous studies (15). Our previous results showed that the average helical content of the centrally labeled 21-aa peptide is about 60% (6, 10), which suggests that the average helical content of the peptides is approximately between 35% (16-mer) and 75% (41-mer). The labels destabilize the helix due to their lower helix propensity compared with Ala (10). Centrally labeled peptides form less stable helices compared with the corresponding N-terminally labeled variants, in agreement with Lifson–Roig theory and previous experimental results (6).

TTET kinetics were monitored by the decay of the xanthone triplet absorbance band at 590 nm. All peptides exhibit double-exponential Xan triplet decay curves, indicating that both the helical state and the coil state are populated to detectable amounts at equilibrium (Fig. 2). An additional very fast kinetic phase is observed within the dead time of the TTET experiments, which is due to fast loop formation in the coil state in a subset of conformations (16). Fig. 2*C* shows that TTET in the central region of the helical peptides becomes slower in longer peptides, whereas TTET in the N-terminal region is virtually independent of peptide length (Fig. 2*G*). The data were fitted using the analytical solution of the three-state model shown in Fig. 1 (*SI Text*) to obtain k_f, k_u, and k_c (10). For all peptides a urea-dependence of the TTET kinetics was measured and the data were fitted globally, which reduces the errors (Fig. S1). Fig. 2 *D* and *H* shows the effect of peptide length on k_f and k_u. Helix formation is independent of peptide length, both in the center (Fig. 2*D*) and at the N terminus (Fig. 2*H*). Helix unfolding in the center, in contrast, becomes slower with increasing peptide length (Fig. 2*D*), whereas unfolding at the N terminus is unchanged (Fig. 2*H*). As a result, increasing peptide length increases helix stability in the central region of the peptide but does not affect helix stability at the N terminus (Table S1). The rate constant for loop formation, k_c, slightly decreases with increasing peptide length (Table S1). This effect is stronger for the centrally labeled peptides compared with the N-terminally labeled peptides, in agreement with our previous results on the effect of tails on the dynamics of loop formation (17).

To compare the experimental results quantitatively with predictions from the kinetic linear Ising model, we performed Monte Carlo simulations as described (10). The simulation procedure was slightly modified to obtain better statistics for the folding and unfolding transitions (*SI Text*). The Monte Carlo simulations yield mean first passage times (FPTs) for helix unfolding and formation in the region between the labels. The rate constants k_f and k_u were determined from the distribution of mean FPTs by fitting the data to a single-exponential decay (Fig. S2). Both in the center and at the N terminus, the simulations yield the same effect of peptide length on k_u, k_f, and K_{eq} as the TTET measurements (Fig. 2 *D* and *H*). The data from experiments and simulations on all centrally labeled peptides can be quantitatively brought into agreement with rate constants for the elementary steps of helix elongation (k_1) and helix shrinking (k_{-1}) of $1.20 \times 10^7\ s^{-1}$ and $1.03 \times 10^7\ s^{-1}$, respectively, which results in an *s*-value of 1.17 ($s = k_1/k_{-1}$) (Eq. **S5** and description of the model in *SI Text*). For the N-terminally labeled peptides, agreement is

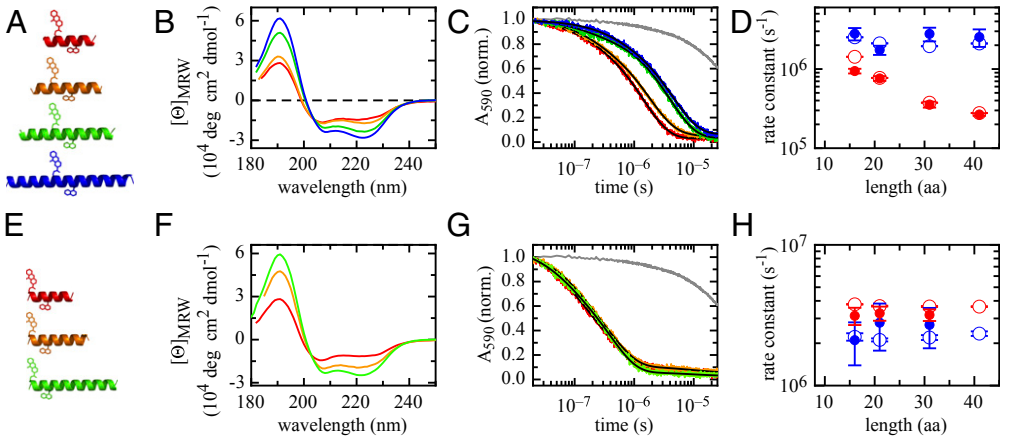

Fig. 2. Effect of peptide length on local helix dynamics and stability. Peptides were labeled with the triplet donor/acceptor pair Xan/Nal either in the center (*A–D*) or at the N terminus (*E–H*). Far-UV CD spectra (*B* and F) and triplet decay curves of xanthone monitored by the change in absorbance at 590 nm (*C* and *G*) are displayed. The colors in the plot correspond to the colors of the helical peptides in *A* and *E*. The gray line represents the triplet decay for a donor-only peptide as a reference. The black lines represent double-exponential fits to the kinetics. A global fit using the analytical solution of the three-state model (Fig. 1) to the data yielded the rate constants for helix formation (k_f), unfolding (k_u), and loop formation (k_c) (*SI Text*). *D* and *H* show the length dependence of k_f (blue) and k_u (red) in the helix center and at the N terminus, respectively. The results are summarized in Table S1. The experimental data (filled circles) agree well with results from Monte Carlo simulation (open circles) based on the linear Ising model (*SI Text*). norm., signal was normalized between 1 (initial absorbance) and 0 (final absorbance); MRW, mean residue weight.

achieved with $k_1 = 1.20 \times 10^7\ s^{-1}$ and $k_{-1} = 9.16 \times 10^6\ s^{-1}$, resulting in an *s*-value of 1.31. The difference in *s*-values between N-terminally and centrally labeled peptides is probably due to the different locations of the labels in the peptide. The TTET labels destabilize the helix more strongly in the center compared with the ends (6), which decreases the average *s*-value used in our simulations. It should be noted that the elementary rate constants k_1 and k_{-1} represent the elementary steps for adding (k_1) and removing (k_{-1}) a single helical segment at the helix/coil boundary in the linear Ising model (Eqs. **S5–S8**). The rate constants k_f and k_u, in contrast, represent the rate constants for helix formation and unfolding in the region between the TTET labels and characterize the transition between conformations that have the helix formed between the labels (H) and conformations allowing TTET (C; Fig. 1).

A T-jump study on helix unfolding found that different *s*-values are required to describe the stability of helical peptides with varying lengths (18). In our study, in contrast, the same *s*-value describes the behavior of the different length peptides, which is in agreement with previous results by Rohl et al. (15) and with the Lifson–Roig model. This discrepancy is likely due to the application of a two-state model to calculate rate constants for helix formation from T-jump unfolding experiments (18), which is not valid because the helix–coil transition is a multistate process (3, 6, 7, 9, 11).

The observed effect of helix length on unfolding dynamics in the peptide center is expected if helix unfolding occurs by 1D diffusion of the helix/coil boundary. Increasing helix length increases the average diffusion distance from the helix/coil boundary to the helix center, and thus the helix/coil boundary takes longer to reach the central region. This mechanism is equivalent to a 1D diffusion process with two boundaries moving, each from one end. To test whether motion of the helix/coil boundary can be described by an Einstein-type, 1D diffusion process, we analyzed the effect of the diffusion distance on the rate constant of helix unfolding. For a classical 1D diffusion mechanism with diffusion from two sides, the survival probability (*S*) for a helical segment in the center can be approximated by an exponential function (*SI Text*):

$$S \approx e^{-\frac{4Dt}{<l^2>}} = e^{-k_u t}, \qquad [1]$$

where *D* represents an upper limit for the diffusion coefficient for one boundary and $<l>$ is the average distance from the helix/coil boundary to the helix center (*SI Text*). Eq. **1** results in a modified Einstein equation for the relationship between the diffusion distance of the boundary and the observed unfolding rate constant (Eq. **2**):

$$<l^2> = \frac{4D}{k_u}. \qquad [2]$$

For the calculation of ($<l>$), we considered that the N- and C-terminal residues are not in a helical conformation (2, 3, 7) and assumed the average helix/coil boundaries at residue 2 and $n-1$ (6, 10). We further assumed that four helical segments between the labels in the center have to unfold for TTET to occur (10). The plot of $<l^2>$ vs. $1/k_u$ is linear (Fig. 3), which shows that helix/coil boundary diffusion in helical peptides follows a classical 1D diffusion law. The slope of the plot yields $D = 3.0{\cdot}10^7$ aa^2/s (Eq. **2**), with $<l>$ given in units of amino acids (aa). The simulations reveal that unfolding in the central region of the helix contains increasing contributions from coil nucleation with increasing helix length, which results in two separate helical segments (Fig. S3). This mechanism occurs in addition to boundary diffusion and increases the observed rate constant for helix unfolding in the central region. The simulations reveal that in the 41-mer, only about 50% of helix unfolding events in the peptide center occur by boundary diffusion of a single helical segment compared with about 95% in the 21-mer (Fig. S3). This result shows

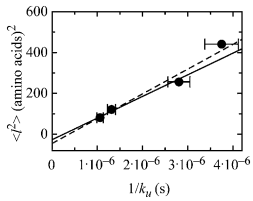

Fig. 3. Correlation between the distance of boundary diffusion and the time constant for helix unfolding. The average diffusion distances, *l*, of the boundaries were calculated between position 2 and the C-terminal label (Nal) for diffusion from the N terminus and between position $n-1$ and the N-terminal label (Xan) for diffusion from the C terminus, and they are given as numbers of amino acids. Data for the centrally labeled peptides shown in Fig. 2 are plotted. The plot of l^2 vs. $1/k_u$ is linear, with a slope of $1.2{\cdot}10^8$ aa^2/s indicating that boundary diffusion can be described by Eq. **1**, with $D = 3.0{\cdot}10^7$ aa^2/s (dashed line). The solid line represents a fit of Eq. **2** to the data for the three shortest helices and yields $D = 2.7{\cdot}10^7$ aa^2/s.

that the single-sequence approximation, which assumes a single contiguous helix (7), does not hold for the unfolding kinetics in the center of the 41-aa peptide. Frequent helix unfolding by coil nucleation in the helix center of the longest helical peptide leads to faster unfolding in the center than expected from the diffusing boundary model. The good agreement between experimental unfolding rate constants and simulations for all peptides indicates that coil nucleation also contributes to the observed TTET kinetics. At equilibrium, however, about 90% of all helices formed in the 41-mer have a single helix, in accordance with the single-sequence approximation (Fig. S3). The comparison between equilibrium and kinetic effects shows that coil nucleation occurs in the center of longer helices but that two isolated helices are not very stable (i.e., they rapidly reform a single helix). The length dependence of k_u for the three shortest peptides, in which boundary diffusion is the dominant process, yields $D = 2.7{\cdot}10^7$ aa^2/s or $6.1{\cdot}10^{-9}$ cm^2/s, with an axial translation of 1.5 Å/aa in a α-helix (Fig. 3). This value is low compared with free diffusion of small molecules and globular proteins. At 5 °C, sucrose has a diffusion coefficient of about $2.5{\cdot}10^{-6}$ cm^2/s and small globular proteins like ribonuclease and lysozyme have diffusion coefficients around $7{\cdot}10^{-7}$ cm^2/s (19). This indicates that boundary diffusion in a α-helix encounters barriers, which are probably due to steric effects and to opening/closing of hydrogen bonds during helix growth and shrinking. Helix boundary diffusion is, however, as fast as the fastest reported 1D diffusion processes of DNA-binding proteins along dsDNA, for which diffusion coefficients in the range of 10^{-12} cm^2/s and 10^{-8} cm^2/s were determined at room temperature, corresponding to a range from 10^3 bp^2/s to 10^7 bp^2/s given in units of base pairs (bp) (20–22).

Effect of Capping Motifs on Helix Stability and Dynamics in the Peptide Center. Specific N- and C-capping motifs are frequently found in protein α-helices (23–25) and were shown to increase helix stability by favorably interacting with the helix dipole (26–28) or by forming side chain-to-backbone hydrogen bonds (25, 29, 30). To investigate the effect of stabilizing the helix termini on helix dynamics in the central region, we made several stabilizing or destabilizing sequence variations at the termini of the 21-aa Ala-based peptide (Table 1). Fig. 4*A* compares the effect of the different N- and C-terminal sequences on global helix stability as judged by the CD signal at 222 nm and reveals large effects on the global helix content (Table S2). Free N or C termini especially lead to major destabilization of the helix, whereas stabilization of the helix dipole by succinylation of the N terminus has a strongly stabilizing effect, as previously observed for the C-peptide derived from the N-terminal helix of RNase A (31).

TTET kinetics in the peptide center become slower with increasing helix stability induced by favorable capping motifs (Fig. 4*B*). The global fit of the urea dependence of the TTET kinetics

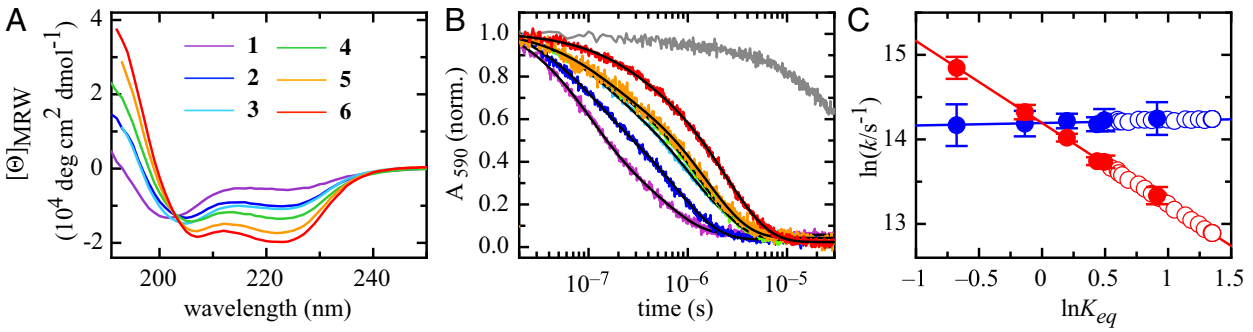

Fig. 4. Effect of end-capping motifs on local dynamics and stability in the peptide center. Local helix–coil dynamics in the center of a 21-aa helical peptide measured by TTET between residues 7 (Xan) and 13 (Nal) are shown. Far-UV CD spectra (*A*) and xanthone triplet decay (*B*) monitored by the absorbance change at 590 nm for peptides with different N- or C-capping motifs are shown. The numbers of the peptides correspond to the numbers in Table 1. The gray line in *B* represents the donor-only reference. The black lines represent double-exponential fits to the data. The results of the fits are given in Table S2. (*C*) Leffler plots helix growth (k_f; blue) and unfolding (k_u; red) (Eq. **3**). Experimental data (closed circles) and results from simulations (open circles) are shown.

(Fig. S4) gave the values of k_f, k_u, k_c, and K_{eq} shown in Table S2. Stabilizing the termini slows down helix unfolding (k_u) in the central region of the peptide but has virtually no effect on helix growth (k_f) leading to helix stabilization in the center. To quantify the effect of changes in helix stability on the folding and unfolding dynamics, we used the Leffler relationship (ϕ-value analysis), which correlates the effect of changes in the free energies of activation of a reaction ($\Delta G^{0\ddagger}$) with the corresponding effect on the equilibrium free energy (ΔG^0) (32–34):

$$\phi_f = \frac{\partial \Delta G_f^{0\ddagger}}{\partial \Delta G^0} = \frac{\partial \ln k_f}{\partial \ln K_{eq}} \quad \phi_u = \frac{\partial \Delta G_u^{0\ddagger}}{\partial \Delta G^0} = \frac{\partial \ln k_u}{\partial \ln K_{eq}} = 1 - \phi_f. \qquad [3]$$

The Leffler plot for the effect of helix capping groups on the rate constants for helix folding/unfolding in the peptide center is shown in Fig. 4*C*. The Leffler plot yields a ϕ_f-value of 0.03 ± 0.16. The error is large due to the errors in the k_f-values, which depend on k_u and on the amplitudes of the fast and slow phases in TTET (Fig. S4). The k_u-values are more accurate, because they are nearly exclusively reflected by the rate constant of the slower observable kinetic phase in TTET (Fig. S4). The corresponding Leffler plot for unfolding yields a ϕ_u-value of 0.97 ± 0.08, confirming the result that only the helix unfolding rate constant (k_u) in the peptide center is affected by changes in the stability at the termini but not the folding rate constant (k_f). All helix capping variants fall on the same line in the Leffler plot, indicating that changes in stability at the N or C terminus have the same effect on helix dynamics, which suggests that boundary diffusion is identical from both directions. The overall stability difference in the central region between the most and least stable helices is only about 2 kJ/mol, which would not yield reliable results in a classical, two-point, ϕ_f-value analysis. However, the use of data from many variants in this stability range increases the accuracy of the analysis (35, 36).

Table 1. Sequence of the α-helical peptides with different capping motifs

No.	Sequence
1	NH_2-AAAAAA**X**ARAAA**Z**RAAAARAA-NH_2
2	NH_2-TAAAAA**X**ARAAA**Z**RAAAARAA-NH_2
3	Ac-AAAAAA**X**ARAAA**Z**RAAAARAA-H
4	Ac-AASAAA**X**ARAAA**Z**RAAAARAA-NH_2
5	Ac-AAAAAA**X**ARAAA**Z**RAAAARAA-NH_2
6	Suc-AAAAAA**X**ARAAA**Z**RAAAARAA-NH_2
7	NH_2-**X**AAAAA**Z**ARAAAARAAAARAA-NH_2
8	Ac-**X**AAAAA**Z**ARAAAARAAAARAA-NH_2
9	Suc-**X**AAAAA**Z**ARAAAARAAAARAA-NH_2

X, Xan attached to Dpr; **Z**, Nal.

These results from TTET experiments were compared with results from the kinetic linear Ising model, with varying local helix stability at the N terminus (*SI Text*). In the simulations, the capping motifs were assumed to change the stability of residues 1–4, which were given the same *s*-value ($s = k_1/k_{-1}$; *SI Text*) between 0.1 and 2. The k_u-, k_f-, and K_{eq}-values in the helix center from the simulations agree well with the experimental results and also give a ϕ_f-value of 0.03 ($\phi_u = 0.97$) (Fig. 4*C*).

In summary, both experiments and simulations show that increasing helix length and stabilizing the terminal regions of a α-helix do not affect the k_f but slow down helix unfolding in the center of a helical peptide. These results demonstrate that nonlocal effects play an important role in modulating the stability and dynamics of α-helices.

Local Effects of Capping Motifs and Amino Acid Sequence on Helix Dynamics and Stability. Local stability of α-helices can be varied by introducing helix-stabilizing or -destabilizing amino acids (30, 37, 38). We synthesized two series of Ala-based 21-aa peptides to investigate the effect of local changes in helix stability on the local folding and unfolding dynamics. In the first series of peptides, we introduced different N-capping motifs and placed the TTET labels at positions 1 and 7 to probe local effects on dynamics and stability in the N-terminal region (Table 1). In the second series, position 10 was varied and the labels were placed at positions 7 and 13, which yields information on local changes in helix stability and dynamics in the center of the peptide.

Varying the N-capping region has only minor effects on the CD spectra of the N-terminally labeled peptides, indicating similar overall helix content (Fig. 5*A*). Despite this small effect on overall helicity, the stabilizing capping groups slow down the TTET kinetics in the N-terminal region (Fig. 5*B*). Global analysis of the urea dependence of the TTET kinetics in the different helices shows that k_f, k_u, and K_{eq} are affected by changes in stability at the N terminus (Table S2). The effect on K_{eq} is as expected from the stabilizing effects of the different capping groups (Table S2). The Leffler plot (Fig. 5*C*) gives a ϕ_f-value of 0.36 ± 0.32 and a corresponding more accurate ϕ_u-value of 0.65 ± 0.11, which yields a ϕ_f-value of 0.35 ± 0.11.

Local dynamics in the N-terminal region of helical peptides were previously measured in T-jump–induced helix unfolding experiments on fluorescence-labeled peptides (9, 39). Both a 4-(methylamino)benzoic acid (MABA) group at the N terminus, which changes its fluorescence on formation of a hydrogen bond to the helix backbone (9), and an i, i + 4 Trp–His interaction at the N terminus (39) gave faster time constants for helix unfolding of about 10 ns at 5 °C and 1 ns at 30 °C, respectively. The faster dynamics compared with TTET-detected helix unfolding may be due to different processes monitored by the different methods.

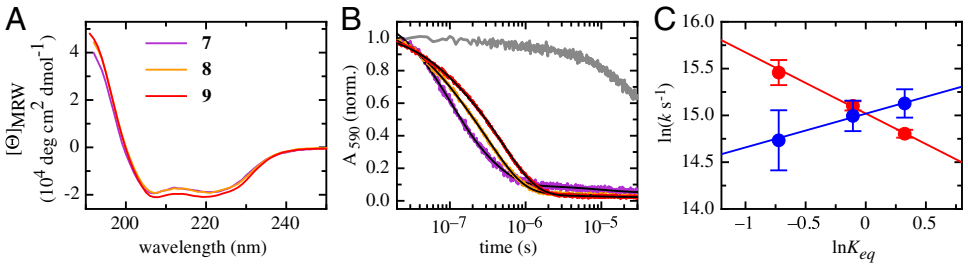

Fig. 5. Effect of N-capping motifs on local helix dynamics and stability at the N terminus. Local helix–coil dynamics at the N terminus of a 21-aa helical peptide measured by TTET between residues 1 (Xan) and 7 (Nal) (Table 1). Far-UV CD spectra (*A*) and xanthone triplet decay (*B*) monitored by the absorbance change at 590 nm are shown. The numbers of the peptides correspond to the numbers in Table 1. The gray line in *B* represents the donor-only reference. The black lines represent double-exponential fits to the kinetics. The results are summarized in Table S2. (*C*) Leffler plots for helix growth (k_f; blue) and unfolding (k_u; red) (Eq. **3**).

TTET requires at least partial unfolding of a 5-aa region between the labels, whereas the fluorescence probes monitor local changes involving the fluorophores, namely, formation of a single hydrogen bond in the case of the MABA label and local opening of a single helical segment at the Trp residue in the Trp–His pair.

Prominent sequence effects on the local dynamics are also observed in the central region of the helical peptides when position 10 is varied (Fig. 6). Host–guest studies on different helical model systems showed that Ala, which is the canonical amino acid at position 10 in the host–guest peptides, is the most helix-stabilizing amino acid, with an *s*-value around 1.5 (30, 37, 38). Thus, any amino acid replacement at position 10 should lead to destabilization of the helix. The short, polar side chains Ser and Thr at position 10 lead to an expected decrease in overall helical content, as judged by the decrease in CD signal at 222 nm (Fig. 6*A* and Table S3). The larger hydrophobic side chains Leu and Ile, in contrast, have only a small effect on the CD signal (Fig. 6*A* and Table S3).

TTET becomes slower in the center of the peptide when local helix stability is increased (Fig. 6*B*). The values for k_f, k_u, and K_{eq} obtained from a global fit of the kinetics at different urea concentrations are shown in Table S3. Interestingly, Leu and Ile at position 10 locally stabilize the center of the helix but leave the overall helical content unchanged (Fig. S4). The Leffler plot for amino acid substitutions at position 10 is complex (Fig. 6*C*). Linear slopes of $\phi_f = 0.33 \pm 0.13$ and $\phi_u = 0.67 \pm 0.07$ are obtained if only linear side chains are considered. These values are similar to the ϕ_f-value observed for local effects in the N-terminal region (Fig. 5*C*). However, k_f and k_u for Val, Ile, Leu, and Thr fall below the lines of the Leffler plots for the linear side chains, indicating that both helix unfolding and folding are slowed down by branched side chains. This observation suggests that branched side chains interfere with both helix folding and unfolding. To test this idea, we introduced the nonnatural amino acids norvaline and norleucine at position 10, which have linear side chains but the same number of methylene groups as Val and Leu/Ile, respectively. Also, norvaline and norleucine at position 10 lead to local stabilization of the helix compared with Ala (Table S3) and to slower TTET kinetics (Fig. 6*B*). In contrast to the branched side chains, k_f and k_u for the nonnatural linear side chains fall onto the same line in the Leffler plot as all other linear amino acids (Fig. 6*C*), indicating that branching is the origin for slower local folding and unfolding dynamics of the helix.

The unexpected helix-stabilizing effect of large hydrophobic side chains at position 10 may be due to stabilizing van der Waals interactions between the side chain at position 10 and the TTET labels. The spacing between each label and position 10 is i, i + 3, which brings them into close vicinity in the helical conformation and may lead to the formation of a hydrophobic helical stair around the helix.

Local and Nonlocal Effects on Helix Dynamics and Stability. Our results demonstrate that amino acid replacements have different effects on local and non-local dynamics and stability of α-helices. Stabilizing the ends of a helix slows down helix unfolding, and thus increases helix stability remote from the region of stabilization. This nonlocal effect can be attributed to longer boundary diffusion distances (Fig. 3). The dynamics of helix formation, in contrast, are not affected by nonlocal changes in helix stability because helix formation monitors a local process, and is thus independent of the position in the helix (10). Changes in helix stability locally affect both helix formation and unfolding with a ϕ_f-value of about 0.35, both at the N terminus and in the helix center. This observation suggests that helix-stabilizing and -destabilizing interactions that lead to different helix propensities for different amino acids influence both elementary steps of helix elongation and shrinking (k_1 and k_{-1} in Eq. **S5**). ϕ_f-Values of about 0.3 are also found for the effect of most mutations on folding of small, single-domain proteins when only reliable ϕ_f-values are considered (36, 40).

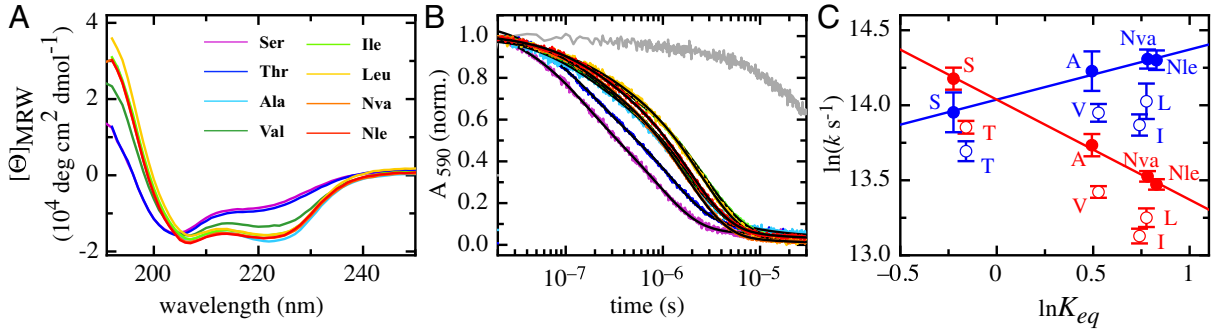

Fig. 6. Effect of amino acid replacements in the peptide center on local helix dynamics and stability in the central region of the peptide. Local helix–coil dynamics in the center of a 21-aa helix measured by TTET between residues 7 (Xan) and 13 (Nal) are shown. Guest amino acids were introduced at position 10. Far-UV CD spectra (*A*) and Xan triplet decay (*B*) monitored by the absorbance change at 590 nm are shown. The gray line in *B* represents the donor-only reference peptide. The black lines represent double-exponential fits to the kinetics. The results are summarized in Table S3. (*C*) Leffler plots for helix growth (k_f; blue) and unfolding (k_u; red) (Eq. **3**). Data for peptides with linear side chains are shown as filled circles, and those for branched side chains are shown as open circles. NLE, norleucine, NVA, norvaline.

For many peptides, the local changes in helix stability measured by TTET do not correlate with the global helix content measured by the CD signal at 222 nm. When the TTET labels are located in the N-terminal region, N-capping motifs have little effect on overall helicity as judged by CD, but they locally increase helix stability at the N terminus (Fig. 5*A*). The helical CD signal at 222 nm was proposed to contain only minor contributions from the N-terminal region, because its amide protons are not involved in hydrogen bonds (41). The center of the 21-aa peptide has a high helical content, independent of the capping sequence. Thus, N caps will mainly affect the helical content in the N-terminal region, which changes the local stability in the N-terminal region but has only little influence on the CD signal at 222 nm. Similarly, helix-stabilizing amino acids in the center of the helices locally increase helix stability but have only little effect on the overall helix content. The central region of a helical peptide has a very high helical content (6, 10). Local stabilization of this region thus only leads to a minor increase in the intensity of the CD band at 222 nm, whereas TTET measurements directly measure local K_{eq}-values, and thus directly give information on local stabilities.

Comparing the effect of N-capping motifs on local helix stability in the helix center (Fig. 4) and in the N-terminal region (Fig. 5) reveals a 1.5-fold stronger effect on the central region (Fig. S5). Stabilizing the helix ends leads to slower unfolding both at the helix ends (Fig. 5) and in the helix center (Fig. 4). However, the effect on k_u in the helix center is larger than at the termini. Stabilizing the helix termini obviously has a strong effect on the efficiency of boundary diffusion. These results show that long-range effects of capping motifs have a strong influence on local stability and unfolding dynamics in distant regions of the helix.

Materials and Methods

All peptides were synthesized and purified as described (10). CD spectra were recorded on an Aviv Circular Dichroism Spectrometer, Model 410, in a 1-mm quartz cuvette at 5 °C. TTET measurements were performed as described (10). In the absence of acceptor, the intrinsic lifetime of the triplet state of a xanthone-only reference helix is about 80 μs. In some TTET traces, an additional phase with less than 5% amplitude and a lifetime corresponding to the donor-only helix is observed. This phase is not considered in further analysis because it is probably due to small amounts of aggregated peptides.

Measurements were performed either in 10 mM potassium phosphate buffer (pH 7) for the length dependence or in 5 mM cacodylic acid (pH 7) at 5 °C for all other experiments. Peptide concentrations were 50 μM and were measured by xanthone absorbance at 343 nm with $\varepsilon = 3{,}900\ M^{-1}{\cdot}cm^{-1}$. Urea concentrations were calculated from the refractive indices (42).

In TTET experiments, between four and eight kinetic traces were recorded. Values of k_f, k_u, and k_c were obtained by globally fitting all kinetic traces at different urea concentrations assuming a linear urea dependence of the logarithms of k_f, k_u, and k_c (10, 43). Equations used for fitting are given in the study by Fierz et al. (10) and in *SI Text*. The program ProFit (Quantum-Soft) was used for data fitting.

ACKNOWLEDGMENTS. We thank Buzz Baldwin and George Rose for comments and discussion, and we thank Attila Szabo for help in deriving Eq. **2**. This work was funded by the Deutsche Forschungsgemeinschaft (SFB 749, A8 and CIPSM).

1. Marqusee S, Robbins VH, Baldwin RL (1989) Unusually stable helix formation in short alanine-based peptides. *Proc Natl Acad Sci USA* 86(14):5286–5290.
2. Zimm BH, Bragg JK (1959) Theory of phase transition between helix and random coil in polypeptide chains. *J Chem Phys* 31(2):526–535.
3. Lifson S, Roig A (1961) On the theory of helix-coil transition in polypeptides. *J Chem Phys* 34(6):1963–1974.
4. Schwarz G, Seelig J (1968) Kinetic properties and the electric field effect of the helix-coil transition of poly(gamma-benzyl L-glutamate) determined from dielectric relaxation measurements. *Biopolymers* 6(9):1263–1277.
5. Gruenewald B, Nicola CU, Lustig A, Schwarz G, Klump H (1979) Kinetics of the helix-coil transition of a polypeptide with non-ionic side groups, derived from ultrasonic relaxation measurements. *Biophys Chem* 9(2):137–147.
6. Chakrabartty A, Schellman JA, Baldwin RL (1991) Large differences in the helix propensities of alanine and glycine. *Nature* 351(6327):586–588.
7. Qian H, Schellman JA (1992) Helix-coil theories: A comparative study for finite length polypeptides. *J Phys Chem* 96(10):3978–3994.
8. Huang CY, Klemke JW, Getahun Z, DeGrado WF, Gai F (2001) Temperature-dependent helix-coil transition of an alanine based peptide. *J Am Chem Soc* 123(38):9235–9238.
9. Thompson PA, Eaton WA, Hofrichter J (1997) Laser temperature jump study of the helix<==>coil kinetics of an alanine peptide interpreted with a 'kinetic zipper' model. *Biochemistry* 36(30):9200–9210.
10. Fierz B, Reiner A, Kiefhaber T (2009) Local conformational dynamics in α-helices measured by fast triplet transfer. *Proc Natl Acad Sci USA* 106(4):1057–1062.
11. Schwarz G (1965) On the kinetics of the helix-coil transition of polypeptides in solution. *J Mol Biol* 11(1):64–77.
12. Krieger F, Fierz B, Bieri O, Drewello M, Kiefhaber T (2003) Dynamics of unfolded polypeptide chains as model for the earliest steps in protein folding. *J Mol Biol* 332(1):265–274.
13. Satzger H, et al. (2004) Ultrafast quenching of the xanthone triplet by energy transfer: new insight into the intersystem crossing kinetics. *J Phys Chem A* 108(46):10072–10079.
14. Heinz B, et al. (2006) On the unusual fluorescence properties of xanthone in water. *Phys Chem Chem Phys* 8(29):3432–3439.
15. Rohl CA, Scholtz JM, York EJ, Stewart JM, Baldwin RL (1992) Kinetics of amide proton exchange in helical peptides of varying chain lengths. Interpretation by the Lifson-Roig equation. *Biochemistry* 31(5):1263–1269.
16. Fierz B, et al. (2007) Loop formation in unfolded polypeptide chains on the picoseconds to microseconds time scale. *Proc Natl Acad Sci USA* 104(7):2163–2168.
17. Fierz B, Kiefhaber T (2007) End-to-end vs interior loop formation kinetics in unfolded polypeptide chains. *J Am Chem Soc* 129(3):672–679.
18. Wang T, et al. (2004) Length dependent helix-coil transition kinetics of nine alanine-based peptides. *J Phys Chem B* 108(39):15301–15310.
19. van Holde KE (1971) *Biophysical Chemistry* (Prentice–Hall, London).
20. Granéli A, Yeykal CC, Robertson RB, Greene EC (2006) Long-distance lateral diffusion of human Rad51 on double-stranded DNA. *Proc Natl Acad Sci USA* 103(5):1221–1226.
21. Wang YM, Austin RH, Cox EC (2006) Single molecule measurements of repressor protein 1D diffusion on DNA. *Phys Rev Lett* 97(4):048302.
22. Blainey PC, et al. (2013) Regulation of a viral proteinase by a peptide and DNA in one-dimensional space: IV. viral proteinase slides along DNA to locate and process its substrates. *J Biol Chem* 288(3):2092–2102.
23. Presta LG, Rose GD (1988) Helix signals in proteins. *Science* 240(4859):1632–1641.
24. Richardson JS, Richardson DC (1988) Amino acid preferences for specific locations at the ends of alpha helices. *Science* 240(4859):1648–1652.
25. Aurora R, Rose GD (1998) Helix capping. *Protein Sci* 7(1):21–38.
26. Hol WGJ (1985) The role of the alpha-helix dipole in protein structure and function. *Prog Biophys Mol Biol* 45:149–195.
27. Shoemaker KR, Kim PS, York EJ, Stewart JM, Baldwin RL (1987) Tests of the helix dipole model for stabilization of α-helices. *Nature* 326(6113):563–567.
28. Sali D, Bycroft M, Fersht AR (1988) Stabilization of protein structure by interaction of alpha-helix dipole with a charged side chain. *Nature* 335(6192):740–743.
29. Doig AJ, Baldwin RL (1995) N- and C-capping preferences for all 20 amino acids in alpha-helical peptides. *Protein Sci* 4(7):1325–1336.
30. Doig AJ, Errington N, Iqbalsyah TM (2005) Stability and design of alpha-helices. *Protein Folding Handbook*, eds Buchner J, Kiefhaber T (Wiley–VCH, Weinheim, Germany), Vol 1, pp 247–313.
31. Shoemaker KR, et al. (1985) Nature of the charged-group effect on the stability of the C-peptide helix. *Proc Natl Acad Sci USA* 82(8):2349–2353.
32. Leffler JE (1953) Parameters for the description of transition states. *Science* 117(3039):340–341.
33. Matouschek A, Kellis JT, Jr., Serrano L, Fersht AR (1989) Mapping the transition state and pathway of protein folding by protein engineering. *Nature* 340(6229):122–126.
34. Sánchez IE, Kiefhaber T (2003) Hammond behavior versus ground state effects in protein folding: Evidence for narrow free energy barriers and residual structure in unfolded states. *J Mol Biol* 327(4):867–884.
35. Northey JG, Maxwell KL, Davidson AR (2002) Protein folding kinetics beyond the phi value: Using multiple amino acid substitutions to investigate the structure of the SH3 domain folding transition state. *J Mol Biol* 320(2):389–402.
36. Sánchez IE, Kiefhaber T (2003) Origin of unusual phi-values in protein folding: evidence against specific nucleation sites. *J Mol Biol* 334(5):1077–1085.
37. Scholtz JM, Baldwin RL (1992) The mechanism of alpha-helix formation by peptides. *Annu Rev Biophys Biomol Struct* 21:95–118.
38. Chakrabartty A, Kortemme T, Baldwin RL (1994) Helix propensities of the amino acids measured in alanine-based peptides without helix-stabilizing side-chain interactions. *Protein Sci* 3(5):843–852.
39. Lin MM, Mohammed OF, Jas GS, Zewail AH (2011) Speed limit of protein folding evidenced in secondary structure dynamics. *Proc Natl Acad Sci USA* 108(40):16622–16627.
40. Naganathan AN, Muñoz V (2010) Insights into protein folding mechanisms from large scale analysis of mutational effects. *Proc Natl Acad Sci USA* 107(19):8611–8616.
41. Gans PJ, Lyu PC, Manning MC, Woody RW, Kallenbach NR (1991) The helix-coil transition in heterogeneous peptides with specific side-chain interactions: Theory and comparison with CD spectral data. *Biopolymers* 31(13):1605–1614.
42. Pace CN (1986) Determination and analysis of urea and guanidine hydrochloride denaturation curves. *Methods Enzymol* 131:266–280.
43. Möglich A, Krieger F, Kiefhaber T (2005) Molecular basis for the effect of urea and guanidinium chloride on the dynamics of unfolded polypeptide chains. *J Mol Biol* 345(1):153–162.